ACS APPLIED MATERIALS & INTERFACES

Research Article

Cite This: ACS Appl. Mater. Interfaces 2018, 10, 38985−38993

www.acsami.org

$HPbI_3$ as a Bifunctional Additive for Morphology Control and Grain Boundary Passivation toward Efficient Planar Perovskite Solar Cells

Yutong He, Wenhui Wang, and Limin Qi*

Beijing National Laboratory for Molecular Sciences (BNLMS), College of Chemistry and Molecular Engineering, Peking University, Beijing 100871, China

Supporting Information

ABSTRACT: One of the key aspects contributing to the rapid development of perovskite solar cells is to prepare high-quality perovskite films via morphology control and interface engineering. Here, we demonstrate that the additive $HPbI_3$ works effectively on both morphology control and grain boundary passivation of $CH_3NH_3PbI_{3-x}Cl_x$ thin films. By inducing $HPbI_3$ to the crystal transformation process, high-quality perovskite films consisting of micro-sized grains with boundaries passivated by PbI_2 can be readily produced. The perovskite film obtained with $HPbI_3$ as the additive achieves a much longer carrier lifetime compared to the pristine perovskite film without the additive. Under the optimal $HPbI_3$ amount (5.0%), the average power conversion efficiency of the planar-heterojunction solar cells is increased by ∼24% to 17.42% from 14.09% for the device without the additive, and the champion efficiency reaches 18.59%. The devices without any encapsulation show impressive shelf stability, retaining more than 85% of the initial efficiency after being stored in ambient environment for over 40 days.

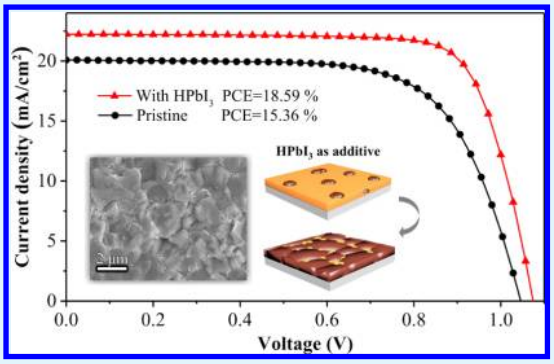

KEYWORDS: *perovskite solar cells, $HPbI_3$, additive, grain size, grain boundary passivation*

1. INTRODUCTION

Organic−inorganic halide perovskite solar cells (PSCs), which are regarded as one of the most promising photovoltaic technologies, have developed rapidly in the past few years, owing to their exceptional optoelectronic properties and convenient preparation methods.[1] The optimization of the fabrication techniques developed since 2009 has resulted in the boosting of the power conversion efficiency (PCE) over 23%.[2] As for the perovskite films prepared by solution-processed methods, the morphology control[3] and interface engineering[4] are crucial for achieving highly efficient and stable PSCs. Tremendous efforts have been focused on developing reproducible approaches toward high-quality perovskite films,[5] which leads to a variety of effective strategies such as coordination engineering,[6] solvent engineering,[7,8] additive engineering,[9] refinements of deposition processes,[10,11] and passivation of grain boundaries (GBs).[12] Among the methods based on precursor solution chemistry, the use of additives has been proven to be advantageous for delicately modulating the perovskite crystallization.[9] In this regard, a series of additives including metal halide salts,[13,14] organic halide salts,[15−17] acids,[18−20] thiols,[21] polymers,[22] surfactants,[23] and nanoparticles[24] have been used for refined control of perovskite crystallization processes. It is noteworthy that urea was recently employed as a bifunctional Lewis base additive to simultaneously enhance crystallinity and passivate defects in perovskite films.[25] Nevertheless, it remains a challenge to explore new bifunctional or multifunctional additives that enable desired control over perovskite crystallization from solutions with various compositions.

It has been reported that hydroiodic acid can assist the fabrication of smooth and pinhole-free perovskite films in either one-step method[26−28] or two-step method.[29] Particularly, HI can reduce the nucleation sites by initiating the dissolution of the lead polyhalide colloids without increasing structural disorder,[30] resulting in larger polycrystalline grain domains with a preferred orientation. Other hydrohalic acids[31−33] and anhydrous hydrogen chloride[34] have also been used to control the crystallization process of perovskite films. Furthermore, HI leads to impressively high solubility of $HPbI_3$ in dimethylformamide (DMF), and hence, the use of the $HPbI_3$ instead of PbI_2 as the precursor compound emerges as an effective strategy to improve perovskite quality. The thus-prepared $HPbI_3$ films were exposed to excess CH_3NH_2 vapor[35,36] or reacted with excess formamidinium iodide[37] to achieve high-quality and stable perovskite films. Similarly, $PbI_2 \cdot x$HI was used to controllably fabricate highly crystallized nonstoichiometry perovskite films via direct gas/solid reaction with CH_3NH_2 gas.[29]

Received: September 6, 2018
Accepted: October 19, 2018
Published: October 19, 2018

DOI: 10.1021/acsami.8b15513
ACS Appl. Mater. Interfaces 2018, 10, 38985−38993

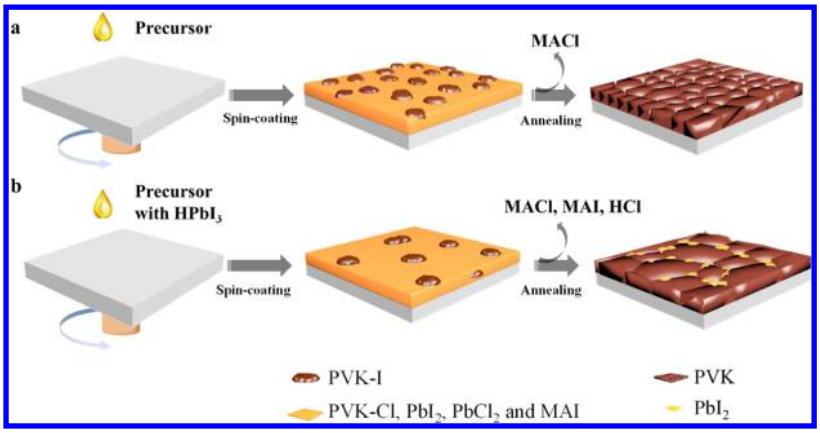

Figure 1. Schematic illustration of the fabrication process of perovskite films (a) without and (b) with additive $HPbI_3$.

On the other hand, both CH_3NH_3I (MAI)[15,38] and PbI_2[39] can act as effective self-doping additives in the precursor solution to treat the GBs of polycrystalline perovskite films. A subtle variation in the organic and inorganic precursor component ratio could significantly affect the crystallinity and bulk carrier lifetimes of perovskite films.[40] What is more, GBs of perovskite films have been generally recognized as recombination sites, leading to the decrease of photovoltaic performance.[4,41] Notably, moderate residual of PbI_2 in the perovskite films could passivate the surface or GB defects and enhance device performance.[12,29,42−44] Therefore, both reducing the number of GBs through increasing grain sizes and passivating GB defects are essential for further enhancement of the cell performance.

Herein, for the first time, we used $HPbI_3$ as a novel bifunctional additive in the perovskite precursor to modulate the crystallization process of organo-lead halide perovskite ($MAPbI_{3-x}Cl_x$) films. The additive $HPbI_3$, which combined the advantageous features of both HI and PbI_2, could lead to not only larger grain sizes of perovskite films but also PbI_2-passivated GBs by influencing the crystallization process and stoichiometry. As a result, the planar-heterojunction PSCs fabricated with $HPbI_3$ as the additive achieved an average PCE of 17.42%, which is much higher than 14.09% for the pristine devices without the additive, and the champion device showed a satisfying PCE of 18.59%. Furthermore, the efficiency can be maintained more than 85% after being stored in air for over 40 days.

2. EXPERIMENTAL SECTION

2.1. Materials. PbI_2 (99.9985%, Alfa Aesar), $PbCl_2$ (99.99%, Aladdin), hydroiodic acid (55−58 wt % in water, contains <1.5% hypophosphorous acid as stabilizer, Aladdin), CH_3NH_2 (30−33 wt % in methanol, Aladdin), titanium isopropoxide (TTIP, 99.999%, Sigma-Aldrich), DMF (99.8%, J&K), 2,2′,7,7′-tetrakis-(*N*,*N*-di-*p*-methoxyphenylamine)-9,9′-spirobifluorene (spiro-OMeTAD, Advanced Election Technology Co., Ltd.), Li-bis-(trifluoromethanesulfonyl)imide (Li-TFSI, >98%, Alfa Aesar), and 4-*tert*-butyl pyridine (96%, J&K) were used as received. All the other chemicals were of analytical grade.

MAI was synthesized and purified in the laboratory. An aqueous HI solution (55−58 wt %) was dropwise added to a solution of methylamine in methanol (30−33 wt %) at a desired stoichiometric ratio in a 100 mL round-bottom flask at 0 °C, which was stirred for 2 h. The resultant precipitate was collected by placing the solution on a rotary evaporator and carefully removing the solvents at 50 °C. Then, the raw product was redissolved in absolute ethanol and recrystallized at room temperature. After filtration, the precipitate was washed with diethyl ether. The resultant white-colored MAI crystals were collected and dried at 60 °C in a vacuum oven for 24 h and used without further purification. 1.125 g PbI_2 and 0.561 g aqueous HI solution (the PbI_2/HI molar ratio was 1:1) were mixed and dissolved in 1.89 g DMF to form a 40 wt % $HPbI_3$ solution. $HPbI_3$ was synthesized according to the literature[35] by heating the 40 wt % $HPbI_3$ solution in DMF at 110 °C in chlorobenzene vapor environment overnight. Light yellow needle-like crystals were washed and dried at 60 °C in a vacuum oven for 24 h.

2.2. Fabrication of Perovskite Thin Films. Fluorine-doped tin oxide (FTO) glass substrates (square resistance 7 Ω, OPV tech Co., China) were patterned by laser etching. The patterned FTO substrates were cleaned by sequentially washing with detergent, deionized water, acetone, and isopropanol. Finally, the FTO substrates were dried by using N_2 flow and treated under the UV−O_3 treatment for 20 min to remove the traces of organic residues. The compact TiO_2 layer used as the electron transport layer was fabricated by spin-coating TTIP solution consisting of 369 μL of TTIP and 40 μL of 2 M HCl in 5.53 mL of ethanol onto the FTO substrates at 5500 rpm for 30 s. Then, the substrates were annealed at 500 °C for 30 min in air.

The pristine perovskite precursor solution without the additive was prepared by dissolving $PbCl_2$, PbI_2, and MAI in DMF, with a molar ratio of 1:1:4, giving a Pb/I molar ratio of 1:3. The concentration of the precursor solutions in DMF was 44 wt %. Subsequently, this solution was stirred and heated at 60 °C overnight in a glovebox (N_2 atmosphere) and different amounts of the additive PbI_2 or $HPbI_3$ [e.g., molar ratios of 3.3, 5.0, and 6.7% with respect to the Pb(II) in the pristine precursor solution] were added. Then, the solution was filtered through a polytetrafluoroethylene filter (0.22 μm).

The resultant perovskite precursor solutions were spin-coated onto the FTO substrates covered by a compact TiO_2 layer at 3000 rpm for 60 s. The poorly crystallized perovskite films obtained were slowly heated from 65 to 85 °C in 20 min with a controlled ramp rate and then kept at 85 °C for 60 min, resulting in well-crystallized perovskite $MAPbI_{3-x}Cl_x$ films. The entire procedure was conducted in the N_2 glovebox.

2.3. Fabrication of Planar PSCs. The hole transport material (HTM) solution was prepared by dissolving 72.3 mg spiro-OMeTAD in 1 mL chlorobenzene, followed by adding 28.8 μL of 4-*tert*-butyl pyridine and 17.5 μL of stock solution of Li-TFSI (520 mg Li-TFSI in 1 mL acetonitrile). After the perovskite films on the TiO_2-coated FTO substrates were cooled down for a few minutes, the HTM solution was spin-coated at 4000 rpm for 30 s. A gold film ∼70 nm in thickness was deposited on the top of the HTM by thermal evaporation with a speed of 1 Å s^{-1}. The area of the PSCs was typically 0.1 cm^2 (0.2 cm × 0.5 cm).

2.4. Instruments and Characterization. Scanning electron microscopy (SEM) images were captured by a field emission scanning electron microscope (Hitachi, S4800, 10 kV) equipped with energy dispersive X-ray spectroscopy (EDS). The absorption spectra were

DOI: 10.1021/acsami.8b15513
ACS Appl. Mater. Interfaces 2018, 10, 38985−38993

obtained by a UV−vis−NIR spectrophotometer (Hitachi, U-4100). The crystal structures were measured by X-ray diffraction (XRD, Philips X pert pro) using Cu Kα radiation. The transient state photoluminescence (PL) spectra at the peak emission of about 783 nm were obtained with a combined lifetime and steady state spectrometer (FLS980, Edinburgh Instruments Ltd.), and the excitation was provided by a picosecond pulsed diode laser (EPL-470, Edinburgh Instruments Ltd.) at the wavelength of 470 nm.

The photocurrent−voltage characteristics of the PSCs were measured by a Keithley model 2400 digital source meter under illumination simulated 100 mW cm^{-2} AM 1.5G irradiation with a solar light simulator (Oriel Instrument, model 94023A) in ambient air. The incident light intensity was calibrated with a NREL-calibrated Si solar cell. The steady state photocurrent generation was measured with a Keithley 4200 system with an Oriel 300 W solar simulator (Thermo Oriel 91160-1000) under illumination simulated 100 mW cm^{-2} AM 1.5G irradiation in a N_2-purged glovebox. The external quantum efficiency (EQE) spectra were measured using a lock-in amplifier coupled with a monochromator (Crowntech, Qtest Station 1000AD).

3. RESULTS AND DISCUSSION

The perovskite $MAPbI_{3-x}Cl_x$ films were fabricated by a one-step deposition technique derived from mixed-lead-halide precursors, which usually involved transformation from chloride-rich intermediate phases.[45,46] The fabrication of the perovskite films was carried out either without additive or with $HPbI_3$ as the additive, as schematically illustrated in Figure 1. For the fabrication of the pristine perovskite films, a precursor solution without the additive was spin-coated on the compact TiO_2-coated substrate, resulting in the formation of both $MAPbI_3$ (PVK-I) and $MAPbCl_3$ (PVK-Cl). Then, PVK-I acted as nucleation centers for reaction of PVK-Cl or $PbCl_2$ with MAI during the subsequent annealing process, leading to the formation of a $MAPbI_{3-x}Cl_x$ (PVK) film with enhanced crystallinity. In contrast, less PVK-I seeds were formed in the presence of the additive $HPbI_3$ because of increased solubility of lead polyhalide colloids in the precursor solution, and the decreased nucleation centers would result in larger grain sizes in the annealed perovskite films. Meanwhile, the volatilization of MACl, MAI, and HCl in the presence of $HPbI_3$ led to residual PbI_2 crystals at the GBs, which could effectively passivate the recombination centers. Therefore, it could be expected that the additive $HPbI_3$ would give rise to larger grains and passivated GBs in the perovskite films, thereby improving the efficiency and stability of the final PSC device.

$HPbI_3$ crystals with high purity were synthesized by the reported antisolvent-crystallization method.[35] The XRD pattern of the obtained crystals displays sharp diffraction peaks at 11.5°, 20.1°, 25.8°, 31.0°, and 35.3° (Figure S1, Supporting Information), which can be ascribed to the (100), (110), (201), (210), and (300) planes of $HPbI_3$, respectively.[36] During the preparation of the perovskite films, we adopted a facile gradient thermal treatment method,[45,47,48] and kept the film annealing at the temperature of 85 °C for 60 min to derive a relatively uniform pinhole-free film. The additive $HPbI_3$ with an amount of 5.0% with respect to the Pb(II) in the pristine precursor solution containing $PbCl_2$, PbI_2, and MAI was added into the precursor solution to tune the crystallization process. For comparison purposes, the precursor solution with 5.0% excess PbI_2 instead of $HPbI_3$ was also used to fabricate perovskite films. The top view SEM images of the perovskite films prepared under different additive conditions are shown in Figure 2. The $MAPbI_{3-x}Cl_x$ film prepared from the pristine precursor exhibits grain sizes of hundreds of nanometers on

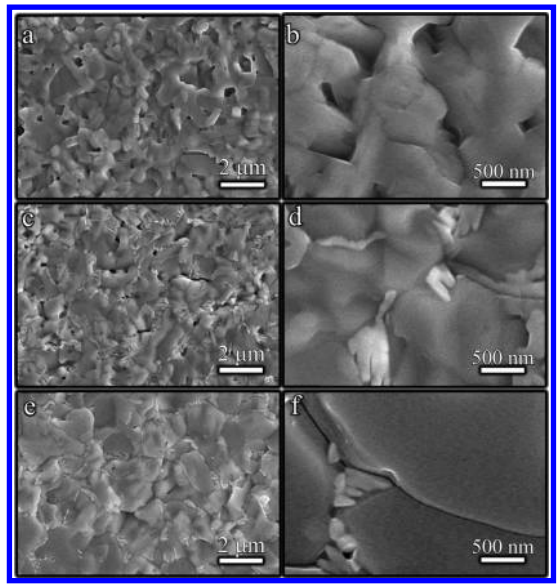

Figure 2. SEM images of perovskite films prepared (a,b) without the additive, (c,d) with additive PbI_2, and (e,f) with additive $HPbI_3$.

account of the existence of chloride (Figure 2a,b), which is consistent with the reported result.[49] The related EDS measurement shows a Cl/I molar ratio of ~0.019 in the resultant $MAPbI_{3-x}Cl_x$ film (Table S1, Supporting Information), indicating a very low content of Cl element in the mixed halide perovskite with $x \approx 0.06$. Comparable grain sizes can be observed in the film with 5.0% excess PbI_2 added in the precursor (Figure 2c,d). In contrast, the perovskite film with 5.0% $HPbI_3$ in the precursor exhibits considerably larger grains with an average size above 1 μm (Figure 2e,f). Interestingly, the GBs of both the perovskite films prepared with excess PbI_2 and with the additive $HPbI_3$ are filled with many small nanoplates showing a higher contrast, which are reminiscent of the small PbI_2 crystals formed around perovskite grains previously reported in the literature.[12,29,42,43] This result strongly indicates that there existed many small PbI_2 crystals at the GBs in the perovskite films because of the volatilization of MACl, MAI, and HCl when the $HPbI_3$ was added in the precursor solution, similar to the case of simple addition of excess PbI_2. The related EDS measurement shows Cl/I molar ratios of ~0.025 and ~0.018 in the resultant $MAPbI_{3-x}Cl_x$ films with PbI_2 and $HPbI_3$, respectively (Table S1, Supporting Information), indicating a very low content of the Cl element in the mixed halide perovskite, similar to the case of the pristine perovskite film.

To obtain the information concerning the crystallinity, light absorption property, defect passivation, and carrier lifetime of the obtained perovskite films, they were further characterized by XRD, UV−vis, and steady-state and time-resolved PL spectra (Figure 3). The XRD patterns shown in Figure 3a suggest that all the three perovskite films show two main reflections located at 14.1° and 28.4°, corresponding to the (110) and (220) planes of mixed halide perovskites, respectively. These two diffraction peaks of the perovskite film with the additive $HPbI_3$ are significantly higher than those for the other two films, suggesting better crystallization, which is in good agreement with the relatively larger grain sizes. It is worth noting that both the perovskite films prepared with excess PbI_2 and the additive $HPbI_3$ exhibit a very weak peak at 12.6° corresponding to the (001) reflection of PbI_2 crystals,

DOI: 10.1021/acsami.8b15513
ACS Appl. Mater. Interfaces 2018, 10, 38985−38993

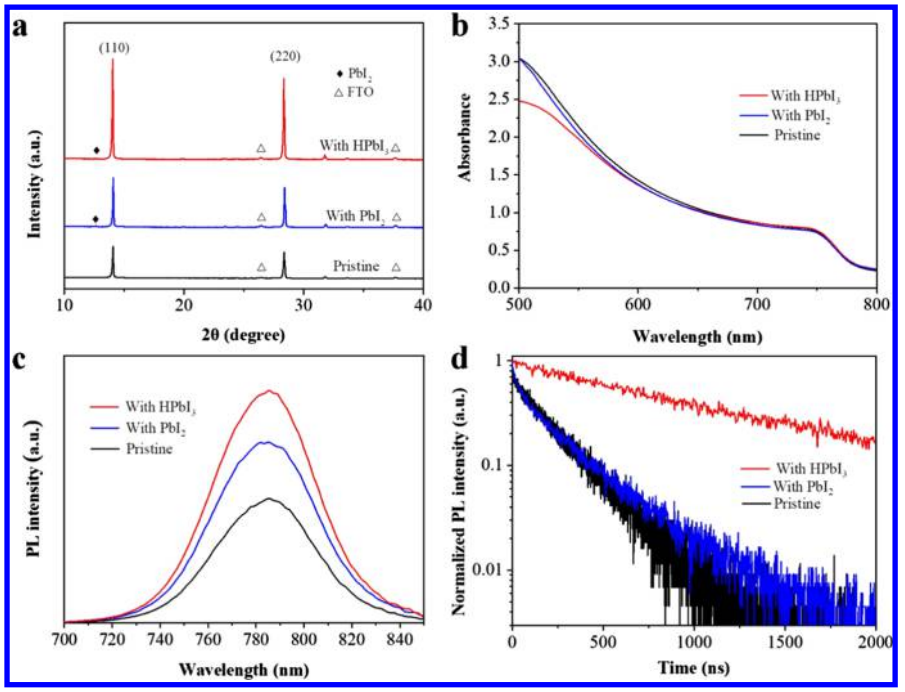

Figure 3. (a) XRD patterns and (b) UV−vis spectra of perovskite films on the FTO substrates. (c) Steady-state PL spectra and (d) time-resolved PL spectra of perovskite films deposited on the glass (excitation at 470 nm).

whereas the pristine perovskite film does not exhibit this peak characteristic of PbI_2, which is consistent with the SEM results shown in Figure 2. This result suggests that in the presence of $HPbI_3$ as the additive, PbI_2 crystals could form near the GBs owing to the volatilization of MACl, MAI, and HCl although the mild annealing process suppressed the formation of PbI_2 in the pristine film prepared from the initial precursor with a Pb/I molar ratio of 1:3. As shown in Figure 3b, all the three perovskite films absorb a wide range of light from the visible to the near-infrared regions with an absorption edge at ∼785 nm, in line with the results previously reported for $MAPbI_{3-x}Cl_x$ films.[46,50] The absorption edge remained essentially unchanged with the addition of PbI_2 and $HPbI_3$, indicating that the band gap of the perovskite was not considerably influenced by the additives in this system.

For the measurements of the steady-state and time-resolved PL spectra, the three perovskite films were prepared on bare glass substrates, which would eliminate the charge injection between the perovskite layer and the electron transfer layer.[53] The PL spectra shown in Figure 3c suggest that all the three films exhibit a strong emission peak at the positions similar to their absorption edges revealed in UV−vis spectra. In comparison with the pristine film, the films with additives show considerable increase in intensity; moreover, the PL intensity of the film with $HPbI_3$ is even higher than that for the film with PbI_2. It is generally recognized that the higher the PL intensity, the fewer the traps or defects in the perovskite films.[51−53] For both the films with PbI_2 and $HPbI_3$, the residual PbI_2 at the GBs would contribute to the passivation of the trap centers, leading to enhanced PL intensity. Moreover, the enlarged grain sizes and increased crystallinity of the film with $HPbI_3$ would give rise to reduced bulk defects, thus further enhancing the PL intensity.[54] The time-resolved PL decays of the three perovskite films are shown in Figure 3d, which can be fitted with a single exponential function. It is shown that the addition of excess PbI_2 can prolong the lifetime of perovskite films from 187.6 to 273.3 ns, owing to the passivation of the GBs or recombination centers by the residual PbI_2, which is consistent with the reported result.[43] Compared with the perovskite film with excess PbI_2, a much longer lifetime (1166.6 ns) is obtained for the film with $HPbI_3$, which can be ascribed to the increased grain sizes and enhanced crystallinity. These results demonstrate that the additive $HPbI_3$ played a key role in simultaneously increasing the grain sizes and passivating the GBs, thus significantly enhancing the optoelectronic quality of the perovskite film.

To figure out the effects of the additive $HPbI_3$ on the crystallization process of the perovskite films, we examined the transformation process from the unannealed films to the final perovskite films by the XRD and SEM measurements. The XRD patterns of the spin-coated films without annealing are shown in Figure 4a, which show weak peaks corresponding to the unreacted PbI_2 and $PbCl_2$ together with two broadened peaks at 14.1° and 28.4°, which can be attributed to the PVK-I. The average crystallite sizes of the PVK-I crystals were estimated from the Scherrer equation using the (220) peak, which suggested that the PVK-I crystals in all the unannealed films were less than ∼40 nm. In addition, a sharp peak at 15.6° can be observed, which could be assigned to PVK-Cl crystals or a mixture of chloride-rich intermediate phases.[55] As documented in the literature,[45,50] homogeneously dispersed PVK-I and PVK-Cl perovskite domains are constructed after spin-coating in the pristine mixed halide system. The rapidly formed PVK-I perovskite serve as "seed" crystals for the sequential transformation of the surrounding PVK-Cl. Furthermore, the less soluble $PbCl_2$ remaining as nanoparticles in solution could provide heterogeneous nucleation sites for the crystallization of PVK-I perovskite crystals.[56] Compared with the pristine film and the film with excess PbI_2, the XRD pattern of the film with the additive $HPbI_3$ exhibits a significantly increased intensity of PVK-Cl relative to PVK-I (110), which may be rationalized by considering that the

DOI: 10.1021/acsami.8b15513
ACS Appl. Mater. Interfaces 2018, 10, 38985−38993

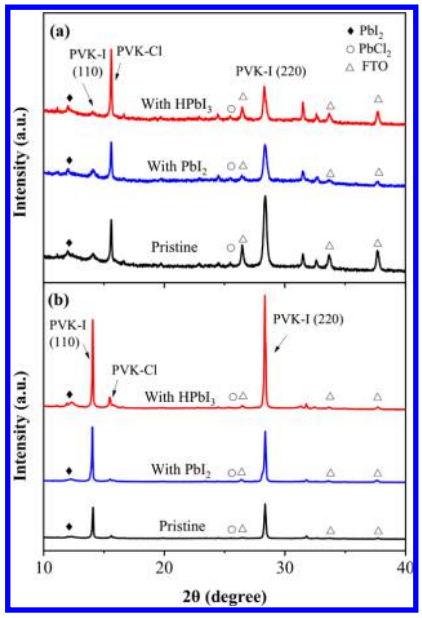

Figure 4. XRD patterns of (a) unannealed films and (b) perovskite films annealed at 85 °C for 10 min.

addition of $HPbI_3$ enhanced the solubility of $PbCl_2$, thereby reducing the PVK-I nucleation sites. The corresponding SEM images of unannealed films suggest that numerous tiny particles with a higher contrast (typically less than 50 nm in size) are distributed in the films (Figure 5a–c). Because the XRD results indicate that PVK-I crystals have average crystallite sizes less than ~40 nm, these tiny particles are reasonably supposed to be the PVK-I crystals. Interestingly, compared with the pristine film and the film with PbI_2, there are considerably less PVK-I crystals on the unannealed film with $HPbI_3$, implying relatively less nucleation sites for the perovskite crystallization upon annealing. After annealing in the glovebox at 85 °C for 10 min, all the three films exhibit significantly increased intensity for PVK-I and concomitant decrease in the intensity of PVK-Cl (Figure 4b), indicating the conversion from PVK-Cl to PVK-I owing to the release of gaseous MACl upon annealing. It may be noted that the film with $HPbI_3$ exhibited the most intensified peaks of PVK-I, indicating the best crystallinity and largest grain sizes resulting from the less nucleation centers in the film with $HPbI_3$. This result is consistent with the SEM observations of the related intermediate perovskite films (Figure 5d–f). After 1 h of annealing at 85 °C, the final mixed halide perovskite films were obtained, as shown in Figure 2, and the perovskite film with $HPbI_3$ exhibited the most desirable features with micro-sized grains and PbI_2-passivated GBs.

To further explore the effects of the additive $HPbI_3$, the perovskite films prepared with varied $HPbI_3$ amounts were characterized by SEM and XRD (Figure S2, Supporting Information). At a lower $HPbI_3$ amount (3.3%), perovskite films with relatively smaller grain sizes were produced, and a few small PbI_2 crystals are visible at the GBs (Figure S2a). When the $HPbI_3$ amount was increased to 5.0%, the grain sizes became larger and the GBs were filled with much more PbI_2 crystals (Figure 2e,f). If the $HPbI_3$ amount was further increased to 6.7%, the grain sizes remained essentially unchanged, and even more PbI_2 crystals accrued at the GBs (Figure S2b), which is consistent with the XRD results (Figures S2c and 3a). Because much residual PbI_2 in the perovskite film is not beneficial for the photovoltaic performance of solar cells, it can be inferred that 5.0% could be the optimum amount of the additive $HPbI_3$ for fabricating high-quality perovskite films with large grain sizes and appropriately passivated GBs. On the other hand, it may be speculated that the additive $HPbI_3$ could be simply replaced by a mixture of HI acid and PbI_2 with a suitable mixing ratio. Therefore, the perovskite films were also prepared by adding an HI/PbI_2 mixture with a similar amount (5.0%); note that the introduction of water to the DMF solution was inevitable in this case because HI was added in the form of aqueous solution of hydroiodic acid. It is known that the impact of water is invariably nonignorable both in the fabrication of perovskite films and in the storage of PSCs.[34,57,58] It can be seen that the perovskite film with the addition of an HI/PbI_2 mixture with a ratio of 1:1 show smaller grain sizes (typically less than 1 μm), and there are no obvious small PbI_2 crystals at the GBs (Figure S3a, Supporting Information). When the HI/PbI_2 ratio was increased to 10:1, the grain sizes become considerably larger due to the presence of a higher concentration of hydroiodic acid, but the small PbI_2 crystals at the GBs are still lacking possibly owing to the introduced water. Therefore, compared with hydroiodic acid or its mixture with PbI_2, a remarkable advantage of the additive $HPbI_3$ is that $HPbI_3$ crystals can be used as a water-free additive to avoid undesirable introduction of water to the perovskite synthesis systems.

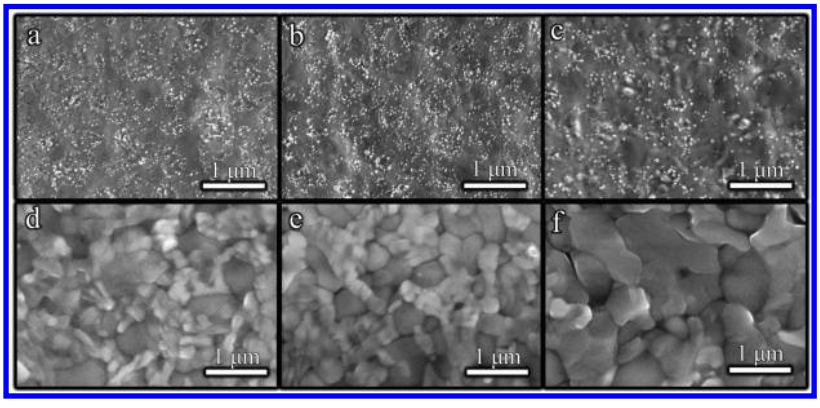

Figure 5. (a–c) SEM images of unannealed films prepared (a) without additive, (b) with PbI_2, and (c) with $HPbI_3$. (d–f) SEM images of perovskite films annealed at 85 °C for 10 min (d) without additive, (e) with PbI_2, and (f) with $HPbI_3$.

DOI: 10.1021/acsami.8b15513
ACS Appl. Mater. Interfaces 2018, 10, 38985–38993

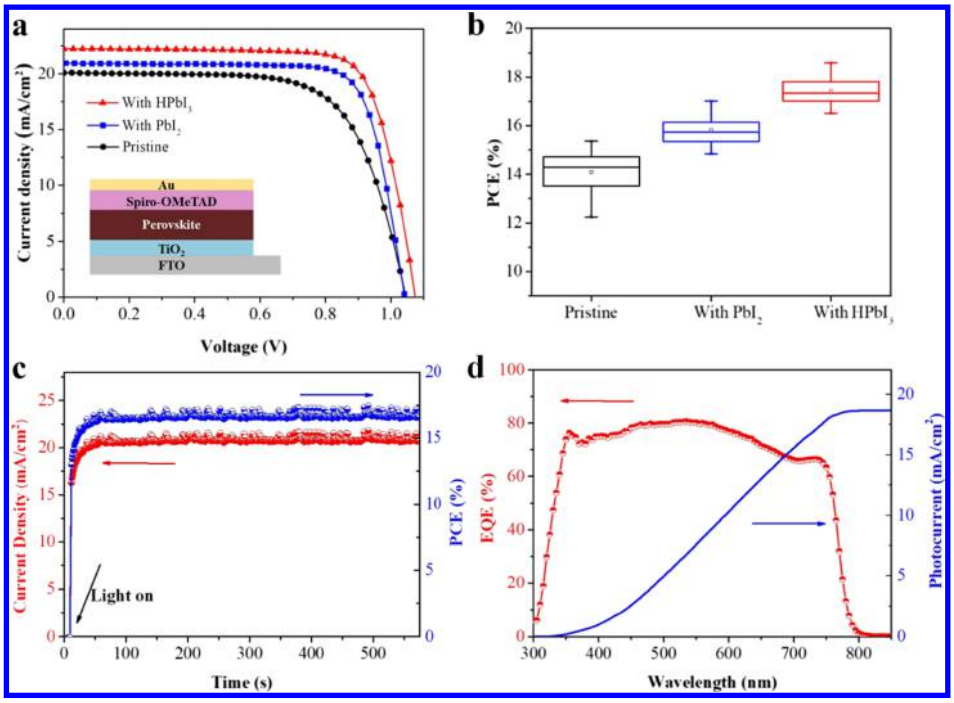

Figure 6. (a) $J-V$ curves of planar PSCs prepared with different additives. (b) PCE of the devices extracted from the $J-V$ measurements for PSCs based on 30 cells for each set. (c) Stabilized output holding the voltage at 0.80 V and (d) EQE spectra of the device prepared with $HPbI_3$.

Table 1. Comparison of Device Performance Parameters for Planar PSCs with Different Additives[a]

				PCE (%)	
samples	V_{OC} (V)	J_{SC} (mA/cm^2)	FF (%)	average	best
with $HPbI_3$	1.05 ± 0.02	21.76 ± 0.67	76.20 ± 1.09	17.42 ± 0.44	18.59
with PbI_2	1.03 ± 0.02	20.84 ± 0.49	74.03 ± 1.91	15.92 ± 0.49	17.02
pristine	0.98 ± 0.04	20.99 ± 0.67	67.83 ± 1.09	14.09 ± 0.70	15.36

[a] V_{OC}, open-circuit voltage; J_{SC}, short-circuit current density; FF, fill factor; PCE, power conversion efficiency (RS); average photovoltaic parameters with standard deviation were obtained based on 30 cells for each set.

Accordingly, a possible mechanism for the fabrication of perovskite films with the additive $HPbI_3$ is tentatively proposed, as is shown in Figure 1. When the pristine perovskite films were prepared without the additive, a precursor film consisting of PVK-I domains surrounded by PVK-Cl and the unreacted PbI_2, $PbCl_2$, and MAI was formed after spin-coating on the substrate. Subsequently, the PVK-I domains acted as nucleation centers for the formation of the mixed halide PVK film with enhanced crystallinity during the annealing process. When $HPbI_3$ was added in the precursor solution, the increased solubility of lead polyhalide colloids in the acid environment would result in reduced PVK-I nucleation centers or suppressed nucleation, leading to larger grain sizes in the annealed perovskite films. Meanwhile, the volatilization of MACl, MAI, and HCl occurred easily due to release of protons from $HPbI_3$ in the solution, resulting in residual PbI_2 crystals near the GBs, which were able to passivate the defects.

The perovskite $MAPbI_{3-x}Cl_x$ films prepared under different additive conditions were fabricated into planar-structured PSC devices. The planar PSCs have the regular cell structure consisting of FTO-coated glass as the substrate, compact TiO_2 as the electron transport layer, perovskite film as the absorber, spiro-OMeTAD as the hole transport layer, and Au as the metal electrode (Figure 6a). These devices possess dense and continuous perovskite films with a thickness of ∼400 nm, resulting from gradient thermal annealing process, as shown in the cross-sectional SEM images of three typical devices (Figure S4, Supporting Information). It can be seen that there are relatively more GBs parallel to the substrate in the perovskite layers of the pristine device without the additive and the device with the additive PbI_2, which is unfavorable for the carrier transport process. The typical current–density voltage ($J-V$) curves of the three planar PSCs under reverse scan are shown in Figure 6a. Thirty individual cells were measured for each kind of device to check the statistics of device performances. The statistical distributions of PCE are shown in Figure 6b and the performance parameters are summarized in Table 1. The pristine solar cell has an average short-circuit current density (J_{SC}) of 20.99 mA cm^{-2}, open-circuit voltage (V_{OC}) of 0.98 V, fill factor (FF) of 67.83%, and PCE of 14.09%. The devices with excess PbI_2 added shows an obvious enhancement in average open-circuit voltage from 0.98 to 1.03 V, which could be associated with the passivation of the GBs by PbI_2. Meanwhile, the excess PbI_2 results in the slight decrease of J_{SC}. When the additive $HPbI_3$ is present in the precursor, the resultant devices show an average J_{SC} of 21.76 mA cm^{-2}, V_{OC} of 1.05 V, FF of 76.20%, and PCE of 17.42%. The increased J_{SC} and FF could be ascribed to the large grain sizes. The residuals at the GBs passivate the trap centers holding up the nonradioactive recombination, which brings about the increased V_{OC}. Thus, the best performing cell achieves a

DOI: 10.1021/acsami.8b15513
ACS Appl. Mater. Interfaces 2018, 10, 38985–38993

PCE of 18.59% when measured under reverse voltage scanning. Because of the hysteretic behavior of the TiO_2-based planar PSCs,[55,59,60] the device with $HPbI_3$ achieves a steady-state efficiency of 16.60% with a steady-state current density of 20.75 mA cm^{-2} at a constant bias voltage of 0.80 V (Figure 6c). As shown in Figure 6d, the EQE spectrum gives an integrating photocurrent density of 18.64 mA cm^{-2}. It may be noted that the current density integrated from the EQE curve is somewhat lower than the J_{SC} value obtained from the $J-V$ curve, which may probably be attributed to the nonlinearities in the recombination mechanism caused by the surface defects on the TiO_2 transporting layer.[34,61−63] Furthermore, the $J-V$ curves of a variety of planar PSCs, which include the PSCs prepared under different additive conditions, with forward and reverse scan directions were displayed (Figure S5, Supporting Information), confirming the close relation between the device performance and the perovskite film morphology. For example, the PCE of the device with $HPbI_3$ was increased with increasing the additive amount from 3.3 to 5.0% on account of enlarged grains and more PbI_2 crystals at the GBs, and then decreased with further increasing the additive amount to 6.7%, owing to a surplus of remaining PbI_2 (Figure S6, Supporting Information).

An air-stable perovskite film is crucial for the long-term stability of PSCs. Preliminary stability investigation on the planar PSCs stored in ambient air (the relative humidity ranged from 20 to 30%) at room temperature without illumination is displayed in Figure 7. The pristine PSC without encapsulation degraded fast, and only ∼60.4% of the initial efficiency was maintained after 42 days. When 5.0% excess PbI_2 was added, the device stability was improved with ∼71.6% of the initial efficiency retained, which was possibly related to the filling of the GBs by PbI_2 crystals as well as somewhat enhanced crystallinity. When 5.0% $HPbI_3$ was added, the device stability was further enhanced because of the much larger grains, which would shield $CH_3NH_3^+$ from moisture,[64] in addition to the filling of the GBs by PbI_2 crystals. As a result, the perovskite film with $HPbI_3$ took an even longer time to degrade. After 42 days of storage in air at room temperature, the devices without encapsulation retained ∼87.8% of the initial PCE, which represents improved shelf stability compared with the previously reported planar PSCs based on $MAPbI_{3-x}Cl_x$ films.[19,50]

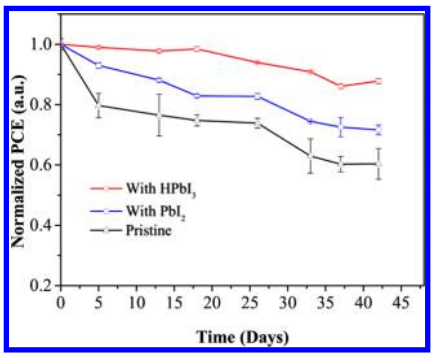

Figure 7. Device stability of the planar PSCs prepared with different additives and stored in ambient atmosphere without illumination. The test was conducted on the devices without encapsulation.

4. CONCLUSIONS

It has been demonstrated that $HPbI_3$ can be used as a novel bifunctional additive to effectively modulate the crystallization process of organo-lead halide perovskite films through simultaneously controlling morphology and passivating GBs. High-quality perovskite films consisting of micro-sized grains with boundaries passivated by PbI_2, which exhibited a much prolonged carrier lifetime, were readily produced in the presence of the additive $HPbI_3$. The planar-heterojunction PSCs fabricated with $HPbI_3$ as the additive achieved an average PCE of 17.42%, which corresponds to ∼24% enhancement compared with the pristine devices, and the champion device exhibited a PCE as high as 18.59%. Furthermore, the efficiency can be maintained more than 85% after being stored in air for over 40 days, indicating an impressive shelf stability. This $HPbI_3$-assisted strategy provides an effective approach for fabricating high-quality perovskite films with desired optoelectronic properties, which may open new avenues toward highly efficient and stable planar PSCs.

■ ASSOCIATED CONTENT

Supporting Information

The Supporting Information is available free of charge on the ACS Publications website at DOI: 10.1021/acsami.8b15513.

Additional XRD patterns, SEM images, EDS results, $J-V$ curves, and PCE data of the perovskite films and PSC devices (PDF)

■ AUTHOR INFORMATION

Corresponding Author

*E-mail: liminqi@pku.edu.cn.

ORCID

Limin Qi: 0000-0003-4959-6928

Notes

The authors declare no competing financial interest.

■ ACKNOWLEDGMENTS

This work was financially supported by NSFC (grant nos. 21473004 and 21673007).

■ REFERENCES

(1) Saliba, M.; Correa-Baena, J.-P.; Grätzel, M.; Hagfeldt, A.; Abate, A. Perovskite Solar Cells: From the Atomic Level to Film Quality and Device Performance. *Angew. Chem., Int. Ed.* **2018**, *57*, 2554−2569.

(2) Jeon, N. J.; Na, H.; Jung, E. H.; Yang, T.-Y.; Lee, Y. G.; Kim, G.; Shin, H.-W.; Il Seok, S.; Lee, J.; Seo, J. A Fluorene-Terminated Hole-Transporting Material for Highly Efficient and Stable Perovskite Solar Cells. *Nat. Energy* **2018**, *3*, 682−689.

(3) Sharenko, A.; Toney, M. F. Relationships between Lead Halide Perovskite Thin-Film Fabrication, Morphology, and Performance in Solar Cells. *J. Am. Chem. Soc.* **2016**, *138*, 463−470.

(4) Bai, Y.; Meng, X.; Yang, S. Interface Engineering for Highly Efficient and Stable Planar p-i-n Perovskite Solar Cells. *Adv. Energy Mater.* **2018**, *8*, 1701883.

(5) Seok, S. I.; Grätzel, M.; Park, N.-G. Methodologies toward Highly Efficient Perovskite Solar Cells. *Small* **2018**, *14*, 1704177.

(6) Yan, K.; Long, M.; Zhang, T.; Wei, Z.; Chen, H.; Yang, S.; Xu, J. Hybrid Halide Perovskite Solar Cell Precursors: Colloidal Chemistry and Coordination Engineering behind Device Processing for High Efficiency. *J. Am. Chem. Soc.* **2015**, *137*, 4460−4468.

(7) Jeon, N. J.; Noh, J. H.; Kim, Y. C.; Yang, W. S.; Ryu, S.; Seok, S. I. Solvent Engineering for High-Performance Inorganic-Organic Hybrid Perovskite Solar Cells. *Nat. Mater.* **2014**, *13*, 897−903.

(8) Bai, Y.; Xiao, S.; Hu, C.; Zhang, T.; Meng, X.; Li, Q.; Yang, Y.; Wong, K. S.; Chen, H.; Yang, S. A Pure and Stable Intermediate Phase is Key to Growing Aligned and Vertically Monolithic Perovskite Crystals for Efficient PIN Planar Perovskite Solar Cells with High Processibility and Stability. *Nano Energy* **2017**, *34*, 58−68.
(9) Li, T.; Pan, Y.; Wang, Z.; Xia, Y.; Chen, Y.; Huang, W. Additive Engineering for Highly Efficient Organic-Inorganic Halide Perovskite Solar Cells: Recent Advances and Perspectives. *J. Mater. Chem. A* **2017**, *5*, 12602−12652.
(10) Chen, J.; Wan, Z.; Liu, J.; Fu, S.-Q.; Zhang, F.; Yang, S.; Tao, S.; Wang, M.; Chen, C. Growth of Compact $CH_3NH_3PbI_3$ Thin Films Governed by the Crystallization in PbI_2 Matrix for Efficient Planar Perovskite Solar Cells. *ACS Appl. Mater. Interfaces* **2018**, *10*, 8649−8658.
(11) Chen, H.; Ding, X.; Xu, P.; Hayat, T.; Alsaedi, A.; Yao, J.; Ding, Y.; Dai, S. Forming Intermediate Phase on the Surface of PbI_2 Precursor Films by Short-Time DMSO Treatment for High-Efficiency Planar Perovskite Solar Cells via Vapor-Assisted Solution Process. *ACS Appl. Mater. Interfaces* **2018**, *10*, 1781−1791.
(12) Jiang, Q.; Chu, Z.; Wang, P.; Yang, X.; Liu, H.; Wang, Y.; Yin, Z.; Wu, J.; Zhang, X.; You, J. Planar-Structure Perovskite Solar Cells with Efficiency beyond 21 %. *Adv. Mater.* **2017**, *29*, 1703852.
(13) Wang, Z.-K.; Li, M.; Yang, Y.-G.; Hu, Y.; Ma, H.; Gao, X.-Y.; Liao, L.-S. High Efficiency Pb-In Binary Metal Perovskite Solar Cells. *Adv. Mater.* **2016**, *28*, 6695−6703.
(14) Bu, T.; Liu, X.; Zhou, Y.; Yi, J.; Huang, X.; Luo, L.; Xiao, J.; Ku, Z.; Peng, Y.; Huang, F.; Cheng, Y.-B.; Zhong, J. A Novel Quadruple-Cation Absorber for Universal Hysteresis Elimination for High Efficiency and Stable Perovskite Solar Cells. *Energy Environ. Sci.* **2017**, *10*, 2509−2515.
(15) Son, D.-Y.; Lee, J.-W.; Choi, Y. J.; Jang, I.-H.; Lee, S.; Yoo, P. J.; Shin, H.; Ahn, N.; Choi, M.; Kim, D.; Park, N.-G. Self-Formed Grain Boundary Healing Layer for Highly Efficient $CH_3NH_3PbI_3$ Perovskite Solar Cells. *Nat. Energy* **2016**, *1*, 16081.
(16) Zhang, X.; Yuan, S.; Lu, H.; Zhang, H.; Wang, P.; Cui, X.; Zhang, Y.; Liu, Q.; Wang, J.; Zhan, Y.; Sun, Z.; Huang, W. Hydrazinium Salt as Additive To Improve Film Morphology and Carrier Lifetime for High-Efficiency Planar-Heterojunction Perovskite Solar Cells via One-Step Method. *ACS Appl. Mater. Interfaces* **2017**, *9*, 36810−36816.
(17) Zhao, Y.; Zhu, K. CH_3NH_3Cl-Assisted One-Step Solution Growth of $CH_3NH_3PbI_3$: Structure, Charge-Carrier Dynamics, and Photovoltaic Properties of Perovskite Solar Cells. *J. Phys. Chem. C* **2014**, *118*, 9412−9418.
(18) Zhang, W.; Pathak, S.; Sakai, N.; Stergiopoulos, T.; Nayak, P. K.; Noel, N. K.; Haghighirad, A. A.; Burlakov, V. M.; deQuilettes, D. W.; Sadhanala, A.; Li, W.; Wang, L.; Ginger, D. S.; Friend, R. H.; Snaith, H. J. Enhanced Optoelectronic Quality of Perovskite Thin Films with Hypophosphorous Acid for Planar Heterojunction Solar Cells. *Nat. Commun.* **2015**, *6*, 10030.
(19) Guo, Y.; Sato, W.; Shoyama, K.; Nakamura, E. Sulfamic Acid-Catalyzed Lead Perovskite Formation for Solar Cell Fabrication on Glass or Plastic Substrates. *J. Am. Chem. Soc.* **2016**, *138*, 5410−5416.
(20) Hou, X.; Huang, S.; Ou-Yang, W.; Pan, L.; Sun, Z.; Chen, X. Constructing Efficient and Stable Perovskite Solar Cells via Interconnecting Perovskite Grains. *ACS Appl. Mater. Interfaces* **2017**, *9*, 35200−35208.
(21) Niu, J.; Yang, D.; Yang, Z.; Wang, D.; Zhu, X.; Zhang, X.; Zuo, S.; Feng, J.; Liu, S. F. Chelate-Pb Intermediate Engineering for High-Efficiency Perovskite Solar Cells. *ACS Appl. Mater. Interfaces* **2018**, *10*, 14744−14750.
(22) Bi, D.; Yi, C.; Luo, J.; Décoppet, J.-D.; Zhang, F.; Zakeeruddin, S. M.; Li, X.; Hagfeldt, A.; Grätzel, M. Polymer-Templated Nucleation and Crystal Growth of Perovskite Films for Solar Cells with Efficiency Greater than 21%. *Nat. Energy* **2016**, *1*, 16142.
(23) Deng, Y.; Zheng, X.; Bai, Y.; Wang, Q.; Zhao, J.; Huang, J. Surfactant-Controlled Ink Drying Enables High-Speed Deposition of Perovskite Films for Efficient Photovoltaic Modules. *Nat. Energy* **2018**, *3*, 560−566.
(24) Li, S.-S.; Chang, C.-H.; Wang, Y.-C.; Lin, C.-W.; Wang, D.-Y.; Lin, J.-C.; Chen, C.-C.; Sheu, H.-S.; Chia, H.-C.; Wu, W.-R.; Jeng, U.-S.; Liang, C.-T.; Sankar, R.; Chou, F.-C.; Chen, C.-W. Intermixing-Seeded Growth for High-Performance Planar Heterojunction Perovskite Solar Cells Assisted by Precursor-Capped Nanoparticles. *Energy Environ. Sci.* **2016**, *9*, 1282−1289.
(25) Lee, J.-W.; Bae, S.-H.; Hsieh, Y.-T.; De Marco, N.; Wang, M.; Sun, P.; Yang, Y. A Bifunctional Lewis Base Additive for Microscopic Homogeneity in Perovskite Solar Cells. *Chem* **2017**, *3*, 290−302.
(26) McMeekin, D. P.; Wang, Z.; Rehman, W.; Pulvirenti, F.; Patel, J. B.; Noel, N. K.; Johnston, M. B.; Marder, S. R.; Herz, L. M.; Snaith, H. J. Crystallization Kinetics and Morphology Control of Formamidinium-Cesium Mixed-Cation Lead Mixed-Halide Perovskite via Tunability of the Colloidal Precursor Solution. *Adv. Mater.* **2017**, *29*, 1607039.
(27) Heo, J. H.; Song, D. H.; Han, H. J.; Kim, S. Y.; Kim, J. H.; Kim, D.; Shin, H. W.; Ahn, T. K.; Wolf, C.; Lee, T.-W.; Im, S. H. Planar $CH_3NH_3PbI_3$ Perovskite Solar Cells with Constant 17.2% Average Power Conversion Efficiency Irrespective of the Scan Rate. *Adv. Mater.* **2015**, *27*, 3424−3430.
(28) Eperon, G. E.; Stranks, S. D.; Menelaou, C.; Johnston, M. B.; Herz, L. M.; Snaith, H. J. Formamidinium Lead Trihalide: a Broadly Tunable Perovskite for Efficient Planar Heterojunction Solar Cells. *Energy Environ. Sci.* **2014**, *7*, 982−988.
(29) Zhang, T.; Guo, N.; Li, G.; Qian, X.; Zhao, Y. A controllable fabrication of grain boundary PbI_2 nanoplates passivated lead halide perovskites for high performance solar cells. *Nano Energy* **2016**, *26*, 50−56.
(30) Sharenko, A.; Mackeen, C.; Jewell, L.; Bridges, F.; Toney, M. F. Evolution of Iodoplumbate Complexes in Methylammonium Lead Iodide Perovskite Precursor Solutions. *Chem. Mater.* **2017**, *29*, 1315−1320.
(31) Heo, J. H.; Song, D. H.; Im, S. H. Planar $CH_3NH_3PbBr_3$ Hybrid Solar Cells with 10.4% Power Conversion Efficiency, Fabricated by Controlled Crystallization in the Spin-Coating Process. *Adv. Mater.* **2014**, *26*, 8179−8183.
(32) Soe, C. M. M.; Stoumpos, C. C.; Harutyunyan, B.; Manley, E. F.; Chen, L. X.; Bedzyk, M. J.; Marks, T. J.; Kanatzidis, M. G. Room Temperature Phase Transition in Methylammonium Lead Iodide Perovskite Thin Films Induced by Hydrohalic Acid Additives. *ChemSusChem* **2016**, *9*, 2656−2665.
(33) Li, G.; Zhang, T.; Zhao, Y. Hydrochloric acid accelerated formation of planar $CH_3NH_3PbI_3$ perovskite with high humidity tolerance. *J. Mater. Chem. A* **2015**, *3*, 19674−19678.
(34) Pan, J.; Mu, C.; Li, Q.; Li, W.; Ma, D.; Xu, D. Room-Temperature, Hydrochloride-Assisted, One-Step Deposition for Highly Efficient and Air-Stable Perovskite Solar Cells. *Adv. Mater.* **2016**, *28*, 8309−8314.
(35) Pang, S.; Zhou, Y.; Wang, Z.; Yang, M.; Krause, A. R.; Zhou, Z.; Zhu, K.; Padture, N. P.; Cui, G. Transformative Evolution of Organolead Triiodide Perovskite Thin Films from Strong Room-Temperature Solid-Gas Interaction between $HPbI_3$-CH_3NH_2 Precursor Pair. *J. Am. Chem. Soc.* **2016**, *138*, 750−753.
(36) Long, M.; Zhang, T.; Chai, Y.; Ng, C.-F.; Mak, T. C. W.; Xu, J.; Yan, K. Nonstoichiometric Acid-Base Reaction as Reliable Synthetic Route to Highly Stable $CH_3NH_3PbI_3$ Perovskite Film. *Nat. Commun.* **2016**, *7*, 13503.
(37) Wang, F.; Yu, H.; Xu, H.; Zhao, N. $HPbI_3$: A New Precursor Compound for Highly Efficient Solution-Processed Perovskite Solar Cells. *Adv. Funct. Mater.* **2015**, *25*, 1120−1126.
(38) Jahandar, M.; Khan, N.; Lee, H. K.; Lee, S. K.; Shin, W. S.; Lee, J.-C.; Song, C. E.; Moon, S.-J. High-Performance $CH_3NH_3PbI_3$-Inverted Planar Perovskite Solar Cells with Fill Factor Over 83% via Excess Organic/Inorganic Halide. *ACS Appl. Mater. Interfaces* **2017**, *9*, 35871−35879.
(39) Roldán-Carmona, C.; Gratia, P.; Zimmermann, I.; Grancini, G.; Gao, P.; Graetzel, M.; Nazeeruddin, M. K. High Efficiency Methylammonium Lead Triiodide Perovskite Solar Cells: the

DOI: 10.1021/acsami.8b15513
ACS Appl. Mater. Interfaces 2018, 10, 38985−38993

Relevance of Non-Stoichiometric Precursors. *Energy Environ. Sci.* **2015**, *8*, 3550−3556.
(40) Yu, H.; Lu, H.; Xie, F.; Zhou, S.; Zhao, N. Native Defect-Induced Hysteresis Behavior in Organolead Iodide Perovskite Solar Cells. *Adv. Funct. Mater.* **2016**, *26*, 1411−1419.
(41) de Quilettes, D. W.; Vorpahl, S. M.; Stranks, S. D.; Nagaoka, H.; Eperon, G. E.; Ziffer, M. E.; Snaith, H. J.; Ginger, D. S. Impact of Microstructure on Local Carrier Lifetime in Perovskite Solar Cells. *Science* **2015**, *348*, 683−686.
(42) Jacobsson, T. J.; Correa-Baena, J.-P.; Halvani Anaraki, E.; Philippe, B.; Stranks, S. D.; Bouduban, M. E. F.; Tress, W.; Schenk, K.; Teuscher, J.; Moser, J.-E.; Rensmo, H.; Hagfeldt, A. Unreacted PbI_2 as a Double-Edged Sword for Enhancing the Performance of Perovskite Solar Cells. *J. Am. Chem. Soc.* **2016**, *138*, 10331−10343.
(43) Chen, Q.; Zhou, H.; Song, T.-B.; Luo, S.; Hong, Z.; Duan, H.-S.; Dou, L.; Liu, Y.; Yang, Y. Controllable Self-Induced Passivation of Hybrid Lead Iodide Perovskites toward High Performance Solar Cells. *Nano Lett.* **2014**, *14*, 4158−4163.
(44) Wang, L.; McCleese, C.; Kovalsky, A.; Zhao, Y.; Burda, C. Femtosecond Time-Resolved Transient Absorption Spectroscopy of $CH_3NH_3PbI_3$ Perovskite Films: Evidence for Passivation Effect of PbI2. *J. Am. Chem. Soc.* **2014**, *136*, 12205−12208.
(45) Cao, C.; Zhang, C.; Yang, J.; Sun, J.; Pang, S.; Wu, H.; Wu, R.; Gao, Y.; Liu, C. Iodine and Chlorine Element Evolution in $CH_3NH_3PbI_3$-xCl_x Thin Films for Highly Efficient Planar Heterojunction Perovskite Solar Cells. *Chem. Mater.* **2016**, *28*, 2742−2749.
(46) Wang, D.; Liu, Z.; Zhou, Z.; Zhu, H.; Zhou, Y.; Huang, C.; Wang, Z.; Xu, H.; Jin, Y.; Fan, B.; Pang, S.; Cui, G. Reproducible One-Step Fabrication of Compact $MAPbI_{3-x}Cl_x$ Thin Films Derived from Mixed-Lead-Halide Precursors. *Chem. Mater.* **2014**, *26*, 7145−7150.
(47) Yang, Y.; Feng, S.; Xu, W.; Li, M.; Li, L.; Zhang, X.; Ji, G.; Zhang, X.; Wang, Z.; Xiong, Y.; Cao, L.; Sun, B.; Gao, X. Enhanced Crystalline Phase Purity of $CH_3NH_3PbI_{3-x}Cl_x$ Film for High-Efficiency Hysteresis-Free Perovskite Solar Cells. *ACS Appl. Mater. Interfaces* **2017**, *9*, 23141−23151.
(48) Fan, B.; Peng, D.; Lin, S.; Wang, N.; Zhao, Y.; Sun, Y. Enhanced Efficiency of Planar-Heterojunction Perovskite Solar Cells through a Thermal Gradient Annealing Process. *RSC Adv.* **2015**, *5*, 58041−58045.
(49) Xu, F.; Zhang, T.; Li, G.; Zhao, Y. Synergetic Effect of Chloride Doping and $CH_3NH_3PbCl_3$ on $CH_3NH_3PbI_{3-x}Cl_x$ Perovskite-Based Solar Cells. *ChemSusChem* **2017**, *10*, 2365−2369.
(50) Zhou, H.; Chen, Q.; Li, G.; Luo, S.; Song, T.-b.; Duan, H.-S.; Hong, Z.; You, J.; Liu, Y.; Yang, Y. Interface Engineering of Highly Efficient Perovskite Solar Cells. *Science* **2014**, *345*, 542−546.
(51) Guo, Y.; Sato, W.; Shoyama, K.; Halim, H.; Itabashi, Y.; Shang, R.; Nakamura, E. Citric Acid Modulated Growth of Oriented Lead Perovskite Crystals for Efficient Solar Cells. *J. Am. Chem. Soc.* **2017**, *139*, 9598−9604.
(52) Zuo, L.; Gu, Z.; Ye, T.; Fu, W.; Wu, G.; Li, H.; Chen, H. Enhanced Photovoltaic Performance of $CH_3NH_3PbI_3$ Perovskite Solar Cells through Interfacial Engineering Using Self-Assembling Monolayer. *J. Am. Chem. Soc.* **2015**, *137*, 2674−2679.
(53) Wu, Y.-H.; Shi, X.-Q.; Ding, X.-H.; Ren, Y.-K.; Hayat, T.; Alsaedi, A.; Ding, Y.; Xu, P.; Dai, S.-Y. Incorporating 4-tert-Butylpyridine in an Antisolvent: A Facile Approach to Obtain Highly Efficient and Stable Perovskite Solar Cells. *ACS Appl. Mater. Interfaces* **2018**, *10*, 3602−3608.
(54) Xiao, S.; Bai, Y.; Meng, X.; Zhang, T.; Chen, H.; Zheng, X.; Hu, C.; Qu, Y.; Yang, S. Unveiling a Key Intermediate in Solvent Vapor Postannealing to Enlarge Crystalline Domains of Organometal Halide Perovskite Films. *Adv. Funct. Mater.* **2017**, *27*, 1604944.
(55) Xu, J.; Fang, M.; Chen, J.; Zhang, B.; Yao, J.; Dai, S. ZnO-Assisted Growth of $CH_3NH_3PbI_{3-x}Cl_x$ Film and Efficient Planar Perovskite Solar Cells with a TiO_2/ZnO/C_{60} Electron Transport Trilayer. *ACS Appl. Mater. Interfaces* **2018**, *10*, 20578−20590.
(56) Tidhar, Y.; Edri, E.; Weissman, H.; Zohar, D.; Hodes, G.; Cahen, D.; Rybtchinski, B.; Kirmayer, S. Crystallization of Methyl Ammonium Lead Halide Perovskites: Implications for Photovoltaic Applications. *J. Am. Chem. Soc.* **2014**, *136*, 13249−13256.
(57) Liu, D.; Traverse, C. J.; Chen, P.; Elinski, M.; Yang, C.; Wang, L.; Young, M.; Lunt, R. R. Aqueous-Containing Precursor Solutions for Efficient Perovskite Solar Cells. *Adv. Sci.* **2018**, *5*, 1700484.
(58) Li, W.; Fan, J.; Mai, Y.; Wang, L. Aquointermediate Assisted Highly Orientated Perovskite Thin Films toward Thermally Stable and Efficient Solar Cells. *Adv. Energy Mater.* **2017**, *7*, 1601433.
(59) Chen, B.; Yang, M.; Priya, S.; Zhu, K. Origin of J-V Hysteresis in Perovskite Solar Cells. *J. Phys. Chem. Lett.* **2016**, *7*, 905−917.
(60) Yang, D.; Zhou, X.; Yang, R.; Yang, Z.; Yu, W.; Wang, X.; Li, C.; Liu, S. F.; Chang, R. P. H. Surface Optimization to Eliminate Hysteresis for Record Efficiency Planar Perovskite Solar Cells. *Energy Environ. Sci.* **2016**, *9*, 3071−3078.
(61) Christians, J. A.; Manser, J. S.; Kamat, P. V. Best Practices in Perovskite Solar Cell Efficiency Measurements. Avoiding the Error of Making Bad Cells Look Good. *J. Phys. Chem. Lett.* **2015**, *6*, 852−857.
(62) Li, L.; Chen, Y.; Liu, Z.; Chen, Q.; Wang, X.; Zhou, H. The Additive Coordination Effect on Hybrids Perovskite Crystallization and High-Performance Solar Cell. *Adv. Mater.* **2016**, *28*, 9862−9868.
(63) Chen, Q.; Zhou, H.; Hong, Z.; Luo, S.; Duan, H.-S.; Wang, H.-H.; Liu, Y.; Li, G.; Yang, Y. Planar Heterojunction Perovskite Solar Cells via Vapor-assisted Solution Process. *J. Am. Chem. Soc.* **2014**, *136*, 622−625.
(64) Wang, Q.; Chen, B.; Liu, Y.; Deng, Y.; Bai, Y.; Dong, Q.; Huang, J. Scaling Behavior of Moisture-Induced Grain Degradation in Polycrystalline Hybrid Perovskite Thin Films. *Energy Environ. Sci.* **2017**, *10*, 516−522.

DOI: 10.1021/acsami.8b15513
ACS Appl. Mater. Interfaces 2018, 10, 38985−38993